IEEE Photonics Journal
An IEEE Photonics Society Publication

Open Access

The Use of Yttria-Alumino-Silicate Bismuth Doped Fibers for Temperature Sensing

Volume 7, Number 4, August 2015

D. Ramirez-Granados
Y. Barmenkov, Member, IEEE
A. Kir'yanov, Member, IEEE
V. Aboites
M. Paul, Member, IEEE
A. Halder
S. Das
A. Dhar
S. Bhadra

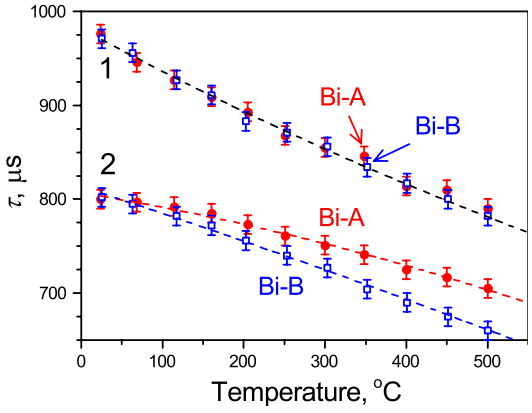

DOI: 10.1109/JPHOT.2015.2447937
1943-0655

IEEE photonics SOCIETY

IEEE

The Use of Yttria-Alumino-Silicate Bismuth Doped Fibers for Temperature Sensing

D. Ramirez-Granados,[1] Y. Barmenkov,[1] *Member, IEEE*, A. Kir'yanov,[1,2] *Member, IEEE*, V. Aboites,[1] M. Paul,[3] *Member, IEEE*, A. Halder,[3] S. Das,[3] A. Dhar,[3] and S. Bhadra[3]

[1]Centro de Investigaciones en Optica, 37150 Leon, Mexico
[2]National University of Science and Technology "MISiS," Moscow 119040, Russia
[3]CSIR-Central Glass and Ceramic Research Institute, Kolkata 700 032, India

DOI: 10.1109/JPHOT.2015.2447937

Manuscript received May 18, 2015; revised June 10, 2015; accepted June 12, 2015. Date of publication June 19, 2015; date of current version July 3, 2015. This work was supported in part by the CONACyT, Mexico, under Project 167945 and Project 242221 and in part by CSIR, India. Corresponding authors: Y. Barmenkov and A. Kir'yanov (e-mail: yuri@cio.mx; kiryanov@cio.mx).

Abstract: Yttria-alumino-silicate fibers heavily doped with bismuth (BI) are investigated for fluorescence temperature sensing within the interval 25 °C . . . 500 °C at 750-nm (LED) excitation. High doping with Bi which resulted in a high concentration of Bi active (fluorescing) centers, is shown to permit the use of short pieces of the fibers as "point" sensors, which is advantageous for applications. Theoretical backgrounds of three commonly utilized sensing techniques, based on measuring fluorescence intensity ratio, fluorescence lifetime, and frequency-domain referencing, are developed and compared, aiming for effective temperature sensing using these fibers.

Index Terms: Fiber temperature sensor, bismuth (Bi)-doped fiber, homogeneous up-conversion, fluorescence-intensity ratio, time-domain fluorescence lifetime, frequency-domain lifetime referencing.

1. Introduction

In the past decade, bismuth (Bi)-doped optical fibers (BDFs) have been attracted much interest as a promising "active" (fluorescing) medium for laser and amplifier applications in a very broad near-infrared (NIR) region ($\sim$1.1 . . . 1.8 μm) at pumping wavelengths ranging from $\sim$450 to $\sim$1500 nm. The choice of a pump wavelength stems from the choice of an absorption band of Bi-related "active" centers (hereafter – BACs) to be matched. It is known that BDFs demonstrate a diversity of BACs, mostly defined by a type of core-glass chemical composition [1]–[9]. Unfortunately, the nature of BACs in different glass hosts responsible for the broadband fluorescence is not yet understood. A separate point of interest regarding BDFs is the effect of temperature [9]–[12] and pump wavelength's variation [1], [4], [9], [13], [14] upon the absorptive and fluorescent properties. It also deserves mentioning that the metastable level's lifetime of BACs in BDFs with different host compositions and at different BACs concentrations varies from $\sim$0.6 to $\sim$1 μs at room temperature [1] and that it decreases with a temperature increase [12].

In the present work, we report the results of an experimental study of the thermal features of NIR fluorescence in new yttria-alumino-silicate fibers heavily doped with Bi in the temperature interval ranging from 25 °C (room temperature) to 500 °C. These BDFs have been drawn from nano-engineered yttria-alumino-silica based preforms and obtained through the Modified Chemical

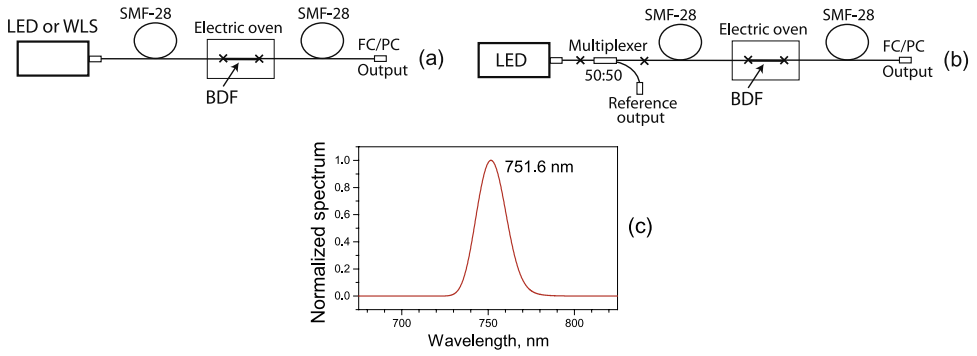

Fig. 1. Experimental arrangements for (a) absorption, fluorescence, and lifetime measurements and (b) for the frequency domain lifetime referencing; crosses indicate the fiber splices; (c) normalized LED spectrum.

Vapor Deposition method in conjunction with the Solution-Doping technique. A detailed analysis of the preforms and fibers of this type is presented in [15]. As follows, we investigate the absorption and fluorescence spectra along with the fluorescence-decay characteristics of these BDFs in function of temperature, with special attention being paid to the effect of BACs concentration (a couple of BDFs with considerably different Bi contents was studied). The results obtained reveal a promise to use such fibers for sensing temperature, which is demonstrated by means of a comparative analysis of three most common techniques to sense temperatures, *viz*., by means of measurements of fluorescence-intensity ratio (FIR) and fluorescence lifetime (FLT), as well as by the frequency-domain lifetime referencing (FDR).

2. Experimental Setups

A set of two BDFs (labeled hereafter Bi-A and Bi-B), doped with Bi ($\sim$0.6 and $\sim$1.0% wt., respectively), also co-doped with Al_2O_3 ($\sim$8.0 wt. %), Y_2O_3 ($\sim$2.5 wt. %), and P_2O_3 (in small amount, $\sim$0.2 wt. %), were handled. Our choice to use the fibers heavily doped with Bi and Al (thus having a high concentration of BACs), was defined by the necessity to operate with short BDF pieces for sensing temperature, which fulfills the requirement of a "point sensor." Co-doping the fibers with Al_2O_3 solved a few tasks: Apart from being a prerequisite for formation of Bi-Al related BACs, this oxide permits easy engineering numerical aperture (NA) of fibers (without a need to add such precursors as Ge) and enhancing chemical durability of the core-glass, which is important for applications, including sensing. In turn, co-doping the fibers with Y_2O_3 targeted facilitating the radiative transitions between the electronic levels of BACs (the phonon energy of Y_2O_3 is one of the lowest cutoffs among oxides [15]–[17]) and, eventually, enhancing the fluorescent ability of BACs in the NIR. Furthermore, adding a small amount of P_2O_5 helped in producing phase-separated particles enriched with Bi and softening of the core-glass.

The absorption coefficients of these two BDFs in the VIS and NIR bands (associated to the presence of BACs) differed by $\sim$3 times (see below). The 1st cutoff wavelengths of Bi-A (lower doped) and Bi-B (heavier doped) fibers were measured to be $\sim$1.5 and $\sim$ 1.4 μm, respectively.

The experimental setups and equipment employed at the measurements are described as follows. The BDF samples were illuminated by a white-light source (WLS, *Yokogawa* AQ4305) for measuring transmission spectra or were pumped by a LED with single-mode fiber output (*Exalos*), for exciting fluorescence [see Fig. 1(a)]. In all experiments described below, BDFs' lengths were fixed, being 4 cm (Bi-A) and 2 cm (Bi-B); therefore, the samples' optical densities at the pump wavelength did not differ much, ensuring a worth comparison of the results obtained with Bi-A and Bi-B fibers. The LED with emission spectrum centered at $\sim$750 nm [see Fig. 1(c)] had a maximum of output power of $\sim$4.5 mW. The LED's output was connected with delivering SMF-28 fiber that was spliced with a BDF sample, spliced, from its other side with another piece of SMF-28 fiber, connected either to a photo-detector (PD), sensitive in IR, or to an optical

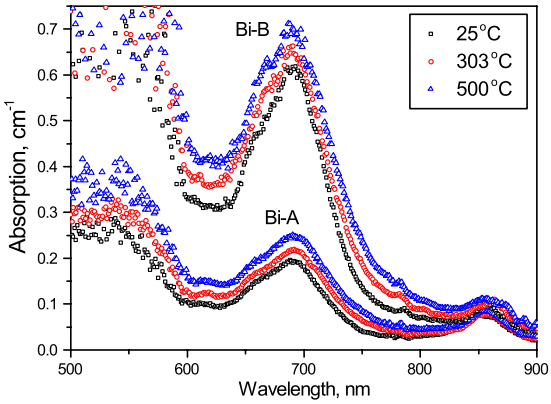

Fig. 2. Absorption spectra of Bi-A and Bi-B fibers at different temperatures.

spectrum analyzer (OSA, *Ando* AQ-6315A). The BDF sample was placed in an electric oven with volume of the isothermal zone of 2 liters, providing temporal stability and accuracy of ± 1 °C and ± 0.5 °C, respectively. The overall resolution of fluorescence lifetime measurements (at applying the FLT sensing technique) was ~ 20 μs. At employing the FDR technique, a 50/50 fused fiber multiplexer, designed for 750 nm, was spliced in between the LED's output and the first piece of SMF-28 fiber [see Fig. 1(b)]; the reference output of the multiplexer served for recording a modulated (by a sinusoid law) signal from the LED.

3. Temperature Effect Upon BDFs' Absorption and Fluorescence Spectra and the FIR Technique's Implementation

First, we studied the absorption spectra of the BDFs at temperatures ranged from 25 °C to 500 °C. This temperature interval was selected because above 500 °C . . . 600 °C, we observed irreversible changes in BDF's core-glass (the effect to be reported elsewhere) and, since the thermal radiation inherent to silica glass gets pronounced beyond 600 °C, exponentially growing at higher temperatures [18], [12].

The attenuation spectra of both BDFs exhibit, between 500 and 900 nm, the two bands centered at ~510 nm and ~700 nm (see Fig. 2), which are the signatures of Bi-Al related BACs; the 3rd—broader but less intensive—absortion band of BACs exists at 1000 . . . 1100 nm. The ~510-nm and ~700-nm bands appear "above" the background loss level, elevating towards shorter wavelengths (a well-known feature for BACs [3], [7], [9], [12], [15], [19]). Note that the peak at ~860 nm and the shoulder on the left side of the ~700-nm band, at ~660 nm, do not relate to Bi but, rather (as discussed in [15]), are the second and third cutoffs of the BDFs (the first cutoff appears at 1400 . . . 1500 nm).

Magnitude of the ~700-nm band was measured to be 0.19 cm^{-1} (Bi-A) and 0.61 cm^{-1} (Bi-B) at room temperature, the difference is ~3 times. As seen from Fig. 2, extinction in this band grows with temperature: for instance, its magnitude at 500 °C is 0.25 cm^{-1} (Bi-A) and 0.69 cm^{-1} (Bi-B), respectively (accordingly, attenuation growth with temperature is measured by ~30% and ~13%). In all the cases, accuracy of the measurements depends on extinction in the bands with standard deviation being ~1% for Bi-A and ~2.5% for Bi-B fibers.

Then, we focused on inspecting the thermally induced changes in NIR fluorescence in the BDFs under pumping by the LED (its operation wavelength, ~750-nm, matches the right slope of the ~700-nm absorption band of BACs). Note that, as the chosen BDF lengths were short enough, this led to a nearly homogenous excitation of the samples. The maximal pump power (4.5 mW) in fluorescence measurements was by ~3.5 dB bigger than the saturation power $P_{sat} = 2.2 \pm 0.2$ mW (for both fibers), characteristic to BACs at this type of excitation; note that P_{sat} was measured at 1200 nm from the BDFs' fluorescence spectra, recorded at different pump powers.

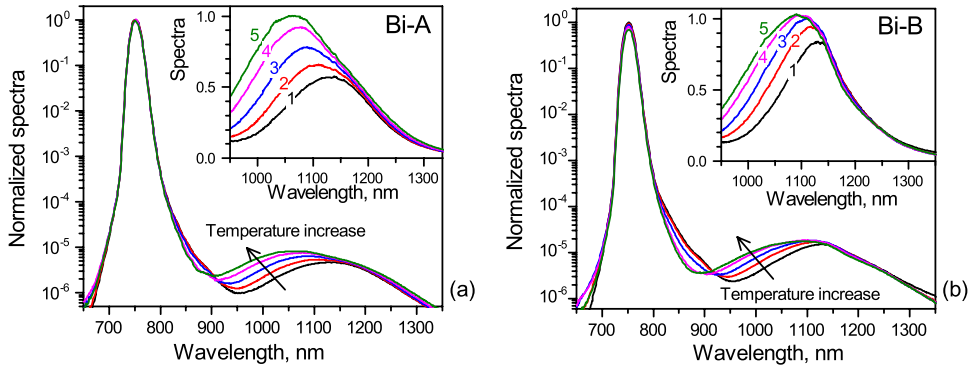

Fig. 3. Spectra of LED and BDFs fluorescence, measured at the output of (a) Bi-A and (b) Bi-B fibers; insets to (a) and (b) show the spectra in a linear scale. Curves from 1 to 5 correspond to temperatures 25 °C, 117 °C, 203 °C, 352 °C, and 500 °C, respectively.

The LED's and BDFs' fluorescence spectra, captured at maximal pump power at different temperatures, are presented in Fig. 3 (the spectra were normalized to the LED's spectral maximum at temperature fixed at 25 °C). At increasing temperature from 25 °C to 500 °C, the LED power at BDF's outputs slightly decreased because of growth of the fibers absorption coefficient at the pump wavelength (from ∼0.04 to ∼0.08 cm^{-1} (Bi-A) and from ∼0.14 to ∼0.24 cm^{-1} (Bi-B)). This led, as seen from Fig. 3, to overall growth of fluorescence power at increasing temperature. Furthermore, a peak of the NIR fluorescence shifted to shorter wavelengths at higher temperatures (which is guided to the eye by arrows in Fig. 3). This can be explained by a thermally induced re-distribution between the lower and upper sub-levels of BACs and by weakening, at a temperature increase, of BACs fluorescence, centered at ∼700 nm [20]. On the other hand, since absorption of both BDFs is measured by ∼1 . . . 10 dB/m (in the 1000 . . . 1100 nm band), for temperatures ranging between 25 °C and 500 °C, the mentioned re-absorption effect does not affect the shape of the fluorescence spectra much, as seen from Fig. 3. Note that a similar trend in fluorescence spectra' modifications at high temperatures was observed in BDFs with a similar composition of core glass at excitation at 1064 nm [11].

The “blue” shift of fluorescence occurring with a temperature increase permits the use of a BDF for temperature sensing by means of the FIR technique. In this technique, the integral power in one part of the fluorescence spectrum is divided on the integral power in its other part [21]; the result (*viz*., the FIR) is a function of temperature, which serves a background for sensing. (Note that a similar procedure was shown to be applicable to sense temperature using glasses doped with semiconductor nanocrystals [22].)

To demonstrate the applicability of the FIR technique for temperature sensing using the BDFs, we handled the fluorescence spectra shown in insets to Fig. 3. The procedure was as follows: the spectra were split into two wavelength intervals, where one ranged from 950 to 1200 nm (A_1) and another—from 1200 to 1500 nm (A_2); an example (for Bi-A fiber at temperature 303 °C) is shown in Fig. 4(a). The “cut wavelength” (see the vertical line in the figure) was chosen to be 1200 nm since at wavelengths beyond the “cut” the fluorescence spectral density varies much less with temperature than below it.

FIR was found, in our case, as the ratio of the areas below the fluorescence spectra (recorded at different temperatures T), $R = A_1/A_2$; the result is presented in Fig. 4(b). As seen from the figure, the FIR-values calculated for both fibers saturate with T growth: the effect also known for rare-earth doped fibers [21]. The absolute sensitivity of the FIR method, $S = dR/dT$, decreases with a temperature increase by a similar manner for the two fibers under study. The S-values were found to vary between room temperature and 500 °C from $\sim 1.16 \times 10^{-2}$ to $\sim 0.29 \times 10^{-2}$ K^{-1}, in case of Bi-A fiber (a four-times drop), and from $\sim 1.47 \times 10^{-2}$ to $\sim 0.24 \times 10^{-2}$ K^{-1}, in case of Bi-B fiber (a six-times drop), correspondingly. In spite of noticeable FIR's dependence on

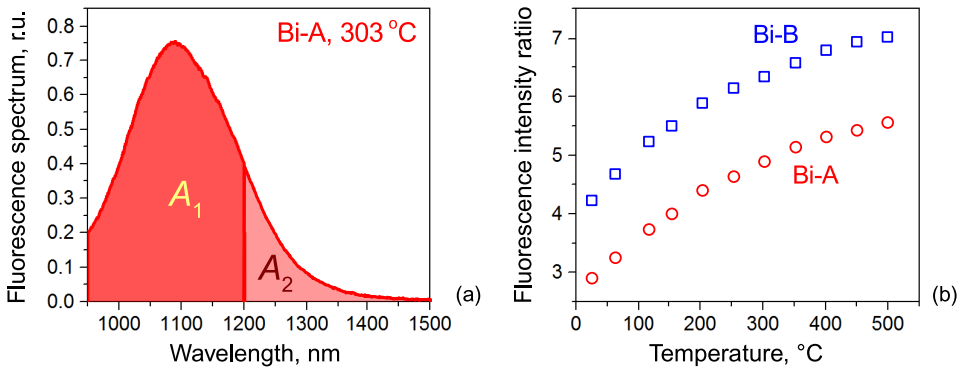

Fig. 4. (a) Fluorescence spectrum of Bi-A fiber (4 cm), measured at 303 °C, which is split into two ranges (A1 and A2), used for the FIR's technique implementation. (b) FIR calculated for Bi-A and Bi-B fibers.

temperature and capability of sensing, this method suffers disadvantages, including i) non-constant sensitivity S within the temperatures domain under study and ii) a necessity of preliminary calibration of a BDF-based sensor prior to sensing. Because of this, we found necessary to study the other methods of sensing temperature with BDFs, based on temporal properties of BACs NIR fluorescence, *viz*., the FLT (time-domain) and FDR (frequency-domain) techniques. As shown below, these two methods demonstrate a virtually constant sensitivity within the temperature range under study.

4. Temperature-Dependent NIR Fluorescence Kinetics: Impact Upon the FLT Method's Applicability

It is known that NIR fluorescence decay deviates from the single-exponent law when the concentration of BACs increases [7], the effect was also observed, for instance, in erbium-doped fibers [23]. Such behavior results from homogenous up-conversion (HUC), i.e., from the energy transfer process between two equivalent centers forming a pair: when both centers occur in the excited state, one of them rapidly decays to the ground state and another one, after fast non-radiative relaxation, remains in the excited state. Thus, HUC results in a non-exponential character of the fluorescence kinetics and can be referred to as fluorescence concentration quenching. In this part, treatment of the HUC-effect and its impact upon measuring temperature-dependent fluorescence decay in BDFs and, correspondingly, upon the FLT method's applicability for sensing temperature are under scope.

The normalized population density n of fluorescing centers (in our case—BACs) in the excited state obeys the following rate equation [19]:

$$\frac{dn}{dt} = -\frac{n}{\tau} - C(n)^2 \tag{1}$$

where $n = N_2/N_0; N_2$ is the population density of BACs in the excited state, N_0 is the overall BACs concentration, τ is the fluorescence lifetime, and C (s^{-1}) is the up-conversion (UC) parameter, defined as product of the "volumetric" HUC constant $C^*(s^{-1}\ cm^3)$ and N_0.

The excitation power should be high enough for establishing a maximal population of the excited state, which is limited by the relation between the ground-state absorption (GSA) and spontaneous-emission cross-sections (σ_{12} and σ_{21}, respectively): The part k of BACs found in the excited state under high-level pumping is defined as $k = \sigma_{12}/(\sigma_{12} + \sigma_{21})$. Assuming that $n(t = 0) = k$ (at pump light switched off at $t = 0$), one can solve (1) analytically [19]:

$$n(t) = k\frac{\exp(-t/\tau)}{1 + (kC)\tau[1 - \exp(t/\tau)]}. \tag{2}$$

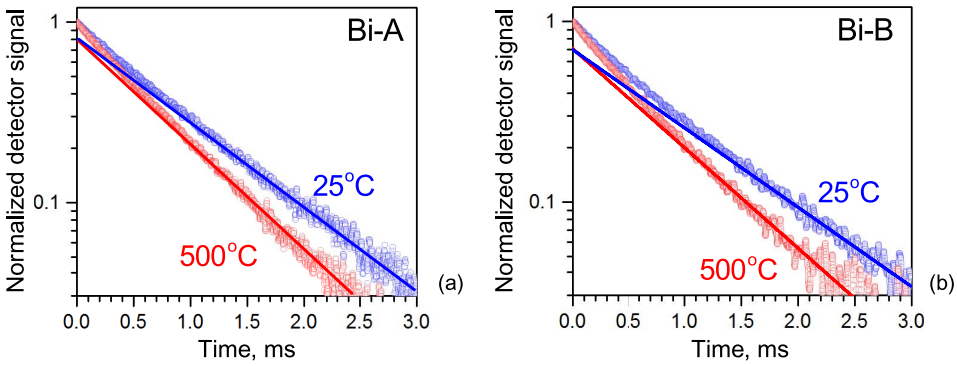

Fig. 5. Fluorescence decays measured at the two extreme temperatures (marked near the curves) (a) for Bi-A and (b) for Bi-B fibers. Points are the experimental data, and solid lines are the exponential fits made for the decays' tails (at $t > 1.5\tau$).

In the absence of HUC ($C = 0$: the case of a low-doped fiber), this formula reduces to the single-exponent law of fluorescence decay.

Formula (2) was used for fitting the experimental data on NIR fluorescence kinetics, obtained for our BDFs within a temperature range 25 °C . . . 500 °C. Consequently, the two key parameters were determined: τ and the product kC (note that in the latter parameter both multiplies generally are temperature-dependent). From (2), one can see that single-exponential decay is observed on a tail of fluorescence decay.

Experimentally, a NIR fluorescence signal was captured after fast switching off pump light; the LED's output power before switching off was fixed at the maximum (4.5 mW). To diminish the pump background contribution in the measured signal, a long-pass optical filter with cut-on wavelength at 1000 nm (*Thorlabs*, model FEL1000) was placed between a BDF's output and Ge-photodetector with 200 kHz bandwidth (*Newport*, model 2033); refer to Fig. 1. Again, we experimented with short pieces of BDFs, that is, 4-cm (Bi-A) and 2-cm (Bi-B), to assess uniformity of pump interaction with fiber.

Fig. 5 shows the examples of fluorescence kinetics, detected for Bi-A and Bi-B fibers, which are seen to significantly deviate from a single exponent. Namely, noticeable discrepancy is observed between the experimental signals and the exponential fits within the interval ranged from $t = 0$ to $t \approx 1.5\tau$ (see the solid lines in the figure), where fluorescence power decreases by about an order of value.

Fig. 6(a) shows the dependencies of NIR fluorescence lifetime obtained using the two kinds of fitting—by single exponent and by (2). One can see that, when the lifetimes are found by the first way (refer to a set of curves labeled 2 in the figure), their values "spread" into two dependencies, with the changes versus temperature being weaker for the less doped Bi-A fiber than for the higher doped Bi-B one. At room temperature, the lifetime values are approximately the same for both fibers ($\sim$800 μs), at this type of fitting. On the other hand, when applying (2) for fitting, the result becomes "merging" of the lifetime dependences in a single curve [labeled 1 in Fig. 6(a)]. It is seen that curve 1 is "shifted up" (by $\sim$200 μs at $t = 0$), as compared to set 2, obtained after fitting by single exponents. At room temperature, the lifetime values obtained as the result of the second kind of fitting become the same ($\sim$975 μs) for both fibers. Notice here that similar values of NIR-fluorescence lifetime at room temperature were recently published [19] for alumino-silicate low-doped BDF upon excitation at 1064 nm.

At fitting the fluorescence lifetime by (2), the product kC (that address the HUC-effect and so applicable to "coupled" BACs) is obtained self-consistently. It stems from (2) that the higher kC-value, the stronger the deviation of fluorescence decay from a single exponent. The kC-values obtained by this way for different temperatures are plotted in Fig. 6(b). It is seen that the product kC is in overall bigger for the heavier doped fiber (Bi-B) and that it steadily grows with temperature, in contrast to the lower doped Bi-A one, for which this trend is imperceptible.

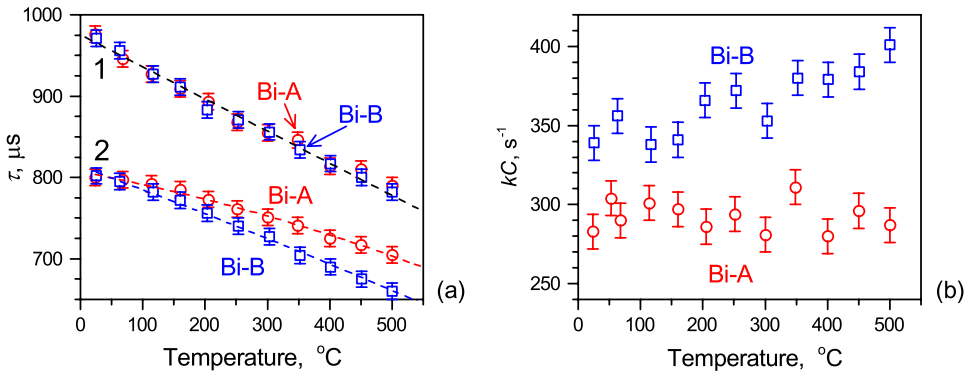

Fig. 6. (a) Fluorescence lifetimes measured for the BDFs in the temperature range from 25 °C to 500 °C. Data 1 demonstrates lifetime values obtained using (2): The circles and squares correspond to Bi-A and Bi-B fibers, respectively (the dash curves fit the experimental points). Data 2 shows the results obtained using the single-exponential law. (b) The product kC as function of temperature.

The FLT method's sensitivity at using BDF as a sensor head is defined by slope of curve 1 in Fig. 6(a), being 0.4 μs/K. Emphasize that this value is found as the result of fitting the fluorescence kinetics by formula (2). This implicitly implies "deliberating" of the HUC phenomenon's impact upon the resultant dependence of lifetime on temperature (taking a linear character once this action has been made). On the contrary, when fluorescence lifetime of BACs is found from a simplified (single-exponent) fitting, the mean sensitivity drops to 0.22 μs/K for Bi-A fiber and to 0.29 μs/K for Bi-B fiber, i.e., it becomes $\sim$30% worse at the least. Moreover, sensitivity in the last case varies with temperature, being smaller at lower temperatures and higher at higher temperatures [see the curves 2 in Fig. 6(a)]. Resuming, fitting the fluorescence decay data by (2), addressing the case of a heavily doped BDF used as a temperature sensor, permits a noticeable increase of the FLT method's sensitivity and, at the same time, ensures linearity of sensing.

5. Sensing Temperature Using the Frequency Domain Lifetime Referencing Method

Actually, the two complementary methods to measure fluorescence lifetime exist, one of them based on the time-domain technique (see above) and the other—on the frequency-domain referencing (FDR) [24]. The second method allows precise determination of fluorescence lifetime using an unsophisticated electronic circuit. Recently, FDR was adapted for a fluorescing medium with two-photon absorption [25] where population inversion of fluorescent centers changes quadratically upon pump power. Hereafter, we discuss another particular but important case of the FDR's implementation, that is, its application to a heavily doped medium with pronounceable HUC.

At FDR, a fluorescing sample is excited by a light source with output power P, modulated by the sinusoidal law at a selected frequency f

$$P_p = P_{p0}(1 + m\sin(2\pi ft)) \tag{3}$$

where P_{p0} is the mean pump power, and m is the pump modulation depth. The fluorescence signal to be detected is modulated at the same frequency (f), its first harmonic is delayed as compared to the modulation signal at the excitation wavelength. The phase difference (delay) between these two signals depends on the fluorescence lifetime that, in turn, is a function of ambient temperature.

To demonstrate the FDR's capacity using a short BDF piece as a sensor head, we utilized the arrangement shown in Fig. 1(b). The LED was modulated by biasing to pump current a sinusoidal AC-component at frequency f. To diminish the LED's power modulation at higher

harmonics of the modulation frequency, the modulation depth was chosen to be not too high ($m = 0.1$). (Another reason for using a low modulation depth is that the formulae for the phase delay obtained below are correct at small modulation depths only.)

Since fluorescence power is a linear function of population inversion of fluorescing centers (in our case—BACs), the relative fluorescence signal is considered further to be proportional to the normalized population density n of BACs being in the excited state [19]:

$$\frac{dn}{dt} = \frac{\sigma_p I_p}{h\nu_p}(1 - n) - \frac{n}{\tau} - Cn^2 \tag{4}$$

where σ_p is the absorption cross-section at the pump wavelength, I_p is the pump intensity, and $h\nu_p$ is the pump photon energy (the other terms have been defined above). The phase delay $\Delta\varphi$ between the modulated LED signal (a reference signal) and the AC-component of the fluorescence signal are obtained analytically for a small pump-modulation depth $(m \ll 1)$:

$$\Delta\varphi = \arctan\left(\frac{\Omega\tau}{\sqrt{(1+s)^2 + 4Cs\tau}}\right) \tag{5}$$

where $\Omega = 2\pi f$ is the modulation circular frequency, and $s = P_{p0}/P_p^{\text{sat}}$ is the mean saturation parameter (here, $P_p^{\text{sat}} = I_p^{\text{sat}} A_p$ is the saturation power, $I_p^{\text{sat}} = (h\nu_p)/(\sigma_p\tau)$ is the saturation intensity at the pump wavelength, and A_p is the geometric square of the pump beam in a BDF). Note that (5) was derived at the assumption of rapid decay of BACs from the pumped level to the metastable (fluorescence-active) one [14]. In the case of a low-doped fiber ($C = 0$), (5) takes the form

$$\Delta\varphi = \arctan\left(\frac{\Omega\tau}{1+s}\right). \tag{6}$$

At very small s-values, this formula reduces to the well-known one (see, e.g., [24])

$$\Delta\varphi = \arctan(\Omega\tau). \tag{7}$$

Let us note that (7) is applicable when the excitation power is "vanishing," which in reality does not hold; therefore, its practical use is not a worthy action in any case. Even though there could be met a situation where this formula is roughly applicable, the fluorescence power (a signal) ought to be tuned down to the values, comparable with background noise of a receiver; apparently, the method's accuracy in this circumstance dramatically drops to a practically irrelevant level. All the said ensures that, instead, the use of (5) and (6), derived above, is a right choice at analyzing the FDR data, at the use of a resonantly absorbing and fluorescing medium with (5) or without (6) account of HUC.

As seen from (5) and (6), the phase delay changes much slower with τ (changing, in turn, with temperature) when the saturation parameter increases; moreover, HUC also effectively reduces the phase change (via parameter C). Thus, one needs to "optimize" the method's sensitivity by making a correct choice of both pump level and modulation frequency, which provide a well-detectable fluorescence signal and, at the same time, not-too-small derivative $d\Delta\varphi/d\tau$ that determines the FDR's sensibility. Another requirement is a preliminary calibration ($\Delta\varphi$ versus temperature T) of a sensor.

In our experiments, the pump power was chosen to be $\approx$1 mW at a BDF's entrance, corresponding to $s \approx 0.5$ in the whole temperature range, the modulation frequency f was fixed at 210 Hz ($\Omega\tau \sim 1$) in the whole lifetime range, and the modulation depth m was fixed at 0.1 (at which the amplitude of pump modulation at the second harmonic of f was $\sim$20-dB less than that at the first harmonic). Similarly to the time-domain measurements (see Section 4), the long-pass optical filter with a cut-on wavelength at 1000 nm, rejecting pump light, was placed in between a BDF's output and InGaAs photo-receiver (*Newport*, model 2053-FC).

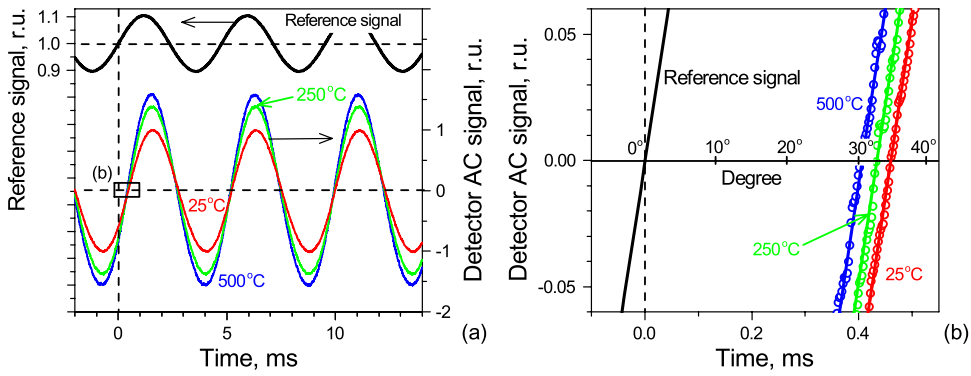

Fig. 7. (a) Signal measured from the reference output and normalized to the mean value (upper curve) and the examples of signals at Bi-B fiber output, captured at 25 °C, 250 °C, and 500 °C. The small square area (b) is zoomed in figure (b). For shorter time scaling, the AC components of these signals, normalized to their amplitudes, are presented: See the three colored curves on the right side (circles show the experimental data and solid lines are their sinusoidal fits). The degree-axis placed at zero of the vertical axis was calculated using (8).

To demonstrate the FDT's capabilities on the example of a BDF-based sensor, we found necessary to show the oscilloscope traces of the detected signals (see Fig. 7), which facilitates understanding of the procedure. The phase shift $\Delta\varphi$ is calculated from the time delay Δt of the signal from the BDF's output [with respect to the signal from the reference output; see Fig. 1(b)], using the relation

$$\Delta\varphi(^\circ) = 360^\circ f \Delta t. \tag{8}$$

The experimental data for one of the fibers (a 2-cm piece of Bi-B fiber, heavier doped with Bi) are plotted in Fig. 7. The long-time traces of the reference signal (the upper black curve) and the normalized AC-components of the fluorescence signal measured at three different temperatures (refer to the lower three different-color curves; normalization was done on the data taken at room temperature) are shown in Fig. 7(a). The short-time traces, featuring the details of measuring $\Delta\varphi$, are presented in Fig. 7(b), which is a zoom of the rectangular box labeled (b) in Fig. 7(a).

As seen from Fig. 7(a) (see the upper trace), the modulation depth of pump power is 10%; note that the value of saturation parameter is $\sim$0.5. It is also seen from the figure that the AC signal's amplitude increases with increasing temperature (see the lower three traces), whereas the delay relatively to the reference signal decreases [see Fig. 7(b)]. The first feature relates to growth of fluorescence power with temperature, see the spectra shown in Fig. 3, while the second one—to drop of the fluorescence lifetime (see Section 4).

Fig. 8 shows the experimental dependences upon temperature of (a) phase shift and (b) amplitude of the first harmonic of the signal, corresponding to fluorescence beyond 1000 nm, measured using Bi-A (red circles) and Bi-B (blue squares) fibers; here, phase shift was obtained by means of relation (8). The experimental dependences of phase shift versus temperature were fitted by (5); the best fits are shown by a set of plain curves 1 in Fig. 8(b). Fitting was proceed for $s = 0.5$ and $m = 0.1$ (the experimental values: see above) at taking the fluorescence lifetimes $\tau(T)$ from the above described temperature-dependent time-domain measurements [see curve 1 in Fig. 6(a)]. The sole parameter subjected to variation at fitting was coefficient C; the fits [dashed curves 1 in Fig. 8(a)] were obtained at C equal to $\sim$400 (Bi-A fiber) and $\sim$550 (Bi-B fiber), respectively. When comparing these values with the above built dependences $kC(T)$ [refer to Fig. 6(b)], one sees that the C-values found after applying the FDR technique are fully compatible with the kC-ones found after applying the FLT technique, at the assumption that k (weakly depending on T) is measured by 0.6...0.65.

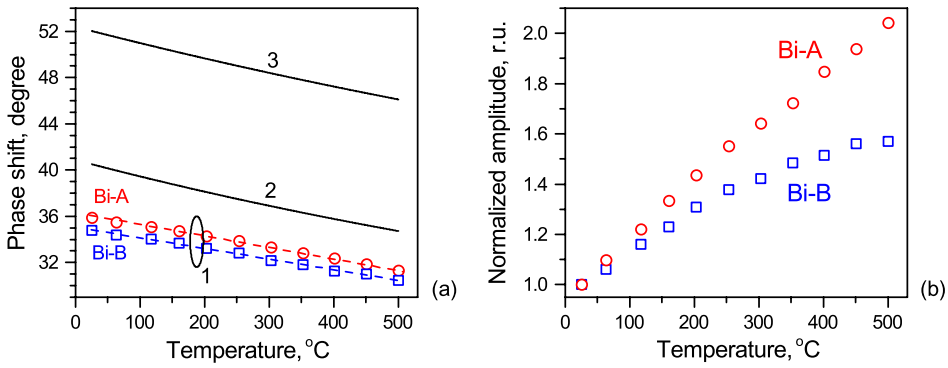

Fig. 8. (a) Phase shift as function of temperature; (b) temperature dependence of amplitude of the first harmonic of BACs fluorescence modulation, normalized to its value at room temperature.

For comparison, we provide in Fig. 8(a) the dependences of phase shift, calculated using formulas (6) (curve 2) and (7) (curve 3); in both cases, calculations were proceed in a similar way, i.e., employing the data on fluorescence lifetime τ versus T [see curve 1 in Fig. 6(a)] and [in case of formula (6)] using $s = 0.5$.

As seen from Fig. 8(a), the two last kinds of modeling fail in attempt to re-construct the experimental dependence of phase shift on temperature (both theoretical curves 2 and 3 lie notably above the experimental data, represented by colored symbols). Specifically, if no saturation (*viz*., at vanishingly low pump power) and no HUC (a low-doped fiber) phenomena are considered [see (7)], the calculated phase shift are the biggest ($\Delta\varphi \sim 46^\circ \ldots 52^\circ$, see curve 3). Further, at taking into account saturation ($s = 0.5$) while presuming none HUC [see (6)], phase shift is found to drop by ~30%, down to $\Delta\varphi \sim 34.7^\circ \ldots 40.5^\circ$, see curve 2). However, the real phase shifts are lower by ~11% (Bi-A) and ~15% (Bi-B) relatively to the latter case, which is a meaningful deviation. The found differences are not surprising, given by rough approximations that these two kinds of modeling imply [especially rough in the case of using (7)], in contrast to capacity of precise fitting that provides modeling by (5).

Thus, at employing the FDR technique for measuring fluorescence lifetime, one should, as demonstrated above, estimate impact of pump-power level (degree of saturation) and possible effect of HUC (inherent to a heavily-doped resonantly-absorbing medium), once seeking a correct interpretation of the experimental data and an appropriate modeling. In this sense, the use of (5), derived above, seems to be the most relevant approach.

Another observation deserving attention is that the mean fluorescence power, captured by the photo-receiver, increases with temperature growth whilst demonstrating “saturating” character for both BDFs [see Fig. 8(b)]. This feature straightforwardly stems from the already noticed (see Fig. 3) enhancement of fluorescent ability of the fibers at increasing temperature. Interestingly, the fluorescence signal in case of Bi-A fiber (lower doped with BACs) “saturates” less than in case of Bi-B one (heavier doped with BAC). However, in spite of this trend, the FDR method's sensibility is seen from Fig. 8(b) to enhance at higher temperatures (due to an effectively larger signal-to-noise factor).

The FDR technique's sensitivity are estimated [see colored curves at bottom of Fig. 8(a)] to be $\sim 9.7 \times 10^{-3}$ and $\sim 9.1 \times 10^{-3}$ degree/K at using, respectively, Bi-A and Bi-B fibers as sensor heads. Therefore, a lower doped BDF is better for sensing temperature as its sensibility is higher [owing to a smaller HUC-constant; see (5)].

6. Conclusion

In this work, the featuring properties of NIR fluorescence in yttria-alumino-silicate fibers heavily doped with Bi (BDFs) at low-power (LED) 750-nm excitation are studied, aiming possible temperature sensing for the 25 °C . . . 500 °C range. The fibers were drawn from the nano-engineered

preforms, made through the Modified Chemical Vapor Deposition method in conjunction with the Solution-Doping technique. The high doping with Bi led to a high concentration of Bi-Al related fluorescence-active centers (BACs), permitting short (a few centimeters in length) pieces of the fibers to be used as sensor's heads ("point sensing"). The most important aspects of a line of the sensing techniques under study—based on measuring fluorescence intensity ratio (FIR), fluorescence lifetime (FLT), and frequency-domain referencing (FDR)—were compared experimentally at using a BDF as a sensor of temperature. In addition, a theoretical background was developed for adequate interpretation of the experimental data collected at implementing the FLT and FDR techniques, with the key novelty being an account of the effects of saturation and homogenous up-conversion (HUC), inherent to heavily doped fibers.

Among the key observations made, mention that, when applying the FIR technique, because of the fact of growth of NIR fluorescence intensity in BDFs at increasing temperature, the FIR-ratio increases, too, but saturates. Moreover, the ratio's saturation trend at high temperatures takes a quantitatively different character at using BDFs with different levels of Bi doping. Another problem at implementing the FIR technique is non-constant sensitivity and a requirement of preliminary calibration of a BDF-based sensor.

The most accurate ways to sense high temperatures using BACs fluorescence were demonstrated to be the FLT and FDR techniques, supplemented by a proper theoretical modeling.

At the FLT, we have demonstrated that for correct determining the NIR fluorescence lifetime one should consider the saturation and HUC (at least for a sensor based on a heavily doped BDF) effects; in this case, fluorescence decay does not obey the exponential law. We gave the analytical formulae that permit easy determining the real fluorescence lifetime, "deliberated" from the HUC effect's contribution in a sophisticated (non-exponential) fluorescence decay and showed applicability of this approach to fit the experimental fluorescence kinetics obtained for both BDFs. As the result, the fluorescence lifetime was demonstrated to be independent of BACs concentration but—which is important for sensor applications—dependent almost linearly on ambient temperature.

At the FDR, we have presented an original approach to determine the fluorescence lifetime when handling a sensor based on a fiber with perceptible HUC in the conditions of fluorescence saturation. In particular, we have demonstrated that, in case of sinusoidal pump modulation, the value of phase shift (or delay) between the reference and fluorescence signals depends not only on fluorescence lifetime and modulation frequency but also on the value of the HUC-constant. Furthermore, we showed—by means of employing the derived analytical algebras—that, when the FDR technique is applied to a heavily doped BDF and when pump power is low enough (a few mW), the phase shift value drops by $\sim$50%, as compared to a hypothetical case of negligible HUC and vanishingly low pump power. At the same time, the slope of the dependence of phase shift on temperature was shown to decrease by $\sim$35%. Needless to say, such details became determinable only as the result of developing a suitable theoretical background for the FDR technique's implementation.

References

[1] E. M. Dianov, "Bismuth-doped optical fibers: A challenging active medium for near-IR lasers and optical amplifiers," *Light: Sci. Appl.*, vol. 1, no. 5, p. e12, May 2012.
[2] E. M. Dianov, "Bi-doped optical fibers: A new active medium for NIR lasers and amplifiers," in *Proc. SPIE*, 2008, vol. 6890, Art. ID. 68900H.
[3] I. A. Bufetov and E. M. Dianov, "Bi-doped fiber lasers," *Laser Phys. Lett.*, vol. 6, no. 7, pp. 487–504, Jun. 2009.
[4] I. Razdobreev *et al.*, "Efficient all-fiber bismuth-doped laser," *Appl. Phys. Lett.*, vol. 90, no. 3, Jan. 2007, Art. ID. 031103.
[5] M. P. Kalita, S. Yoo, and J. Sahu, "Bismuth-doped fiber laser and study of unsaturable loss and pump induced absorption in laser performance," *Opt. Exp.*, vol. 16, no. 25, pp. 21 032–21 038, Dec. 2008.
[6] V. G. Truong, L. Bigot, A. Lerouge, M. Douay, and I. Razdobreev, "Study of thermal stability and luminescence quenching properties of bismuth-doped silicate glasses for fiber laser applications," *Appl. Phys. Lett.*, vol. 92, no. 4, Jan. 2008, Art. ID. 041908.

[7] V. V. Dvoyrin *et al.*, "Absorption, gain and laser action in bismuth-doped aluminosilicate optical fibers," *IEEE J. Quantum Electron.*, vol. 46, no. 2, pp. 182–189, Feb. 2010.
[8] E. M. Dianov *et al.*, "A new bismuth-doped fibre laser, emitting in the range 1625–1775 nm," *Quantum Electron.*, vol. 44, no. 6, pp. 503–504, Jun. 2014.
[9] I. A. Bufetov *et al.*, "Bi-doped optical fibers and fiber lasers," *IEEE Sel. Topics Quantum Electron.*, vol. 20, no. 5, Sep./Oct. 2014, Art. ID. 0903815.
[10] S. V. Firstov *et al.*, "Combined excitation–emission spectroscopy of bismuth active centers in optical fibers," *Opt. Exp.*, vol. 19, no. 20, pp. 19 551–19 561, Sep. 2011.
[11] V. V. Dvoyrin, V. M. Mashinsky, and E. M. Dianov, "Efficient bismuth-doped fiber lasers," *IEEE J. Quantum Electron.*, vol. 44, no. 9, pp. 834–839, Sep./Oct. 2008.
[12] D. A. Dvoretskii *et al.*, "Optical properties of bismuth-doped silica fibres in the temperature range 300–1500 K," *Quantum Electron.*, vol. 42, no. 9, pp. 762–769, 2012.
[13] I. Razdobreev *et al.*, "Optical properties of bismuth-doped silica core photonic crystal fiber," *Opt. Exp.*, vol. 18, no. 19, pp. 19 479–19 484, Sep. 2010.
[14] S. Yoo, M. P. Kalita, J. Nilsson, and J. Sahu, "Excited state absorption measurement in the 900–1250 nm wavelength range for bismuth-doped silicate fibers," *Opt. Lett.*, vol. 34, no. 4, pp. 530–532, Feb. 2009.
[15] A. V. Kir'yanov *et al.*, "Distribution of bismuth and bismuth-related centers in core area of $Y-Al-SiO_2$: Bi fibers," *J. Lightw. Technol.*, to be published. [Online]. Available: http://ieeexplore.ieee.org/xpl/login.jsp?tp=arnumber=urlttp%3A%2F%2Fieeexplore.ieee.org%2Fxpls%2Fabs_all.jsp%3Farnumber%3D7131439
[16] M. Hughes, T. Suzuki, and Y. Ohishi, "Compositional optimization of bismuth-doped yttria-alumina-silica glass," *Opt. Mater.*, vol. 32, no. 2, pp. 368–373, Dec. 2009.
[17] Q. Qian, Q. Y. Zhang, G. F. Yang, Z. M. Yang, and Z. H. Jiang, "Enhanced broadband near-infrared emission from Bi-doped glasses by codoping with metal oxides," *J. Appl. Phys.*, vol. 104, no. 4, Aug. 2008, Art. ID. 043518.
[18] E. Haro-Poniatowski *et al.*, "Size-dependent thermo-optical properties of embedded Bi nanostructures," *Nanotechnol*, vol. 19, no. 48, Dec. 2008, Art. ID. 485708.
[19] A. V. Kir'yanov, V. V. Dvoyrin, V. M. Mashinsky, Y. O. Barmenkov, and E. M. Dianov, "Nonsaturable absorption in alumino-silicate bismuth-doped fibers," *J. Appl. Phys.*, vol. 109, no. 2, Jan. 2011, Art. ID. 023113.
[20] L. I. Bulatov *et al.*, "Structure of absorption and luminescence bands in aluminosilicate optical fibers doped with bismuth," *Bull. Russian Acad. Sci.*, vol. 72, no. 12, pp. 1655–1660, Dec. 2008.
[21] S. A. Wade, S. F. Collins, and G. W. Baxter, "Fluorescence intensity ratio technique for optical fiber point temperature sensing," *J. Appl. Phys.*, vol. 94, no. 8, pp. 4743–4756, Oct. 2003.
[22] C. Sifuentes, Y. O. Barmenkov, A. N. Starodumov, V. N. Filippov, and A. A. Lipovskii, "Application of CdSe-nanocrystallite-doped glass for temperature measurements in fiber sensors," *Opt. Eng.*, vol. 39, no. 8, pp. 2182–2186, Aug. 2000.
[23] A. V. Kir'yanov, Y. O. Barmenkov, G. E. Sandoval-Romero, and L. Escalante-Zarate, "Er^{3+} concentration effects in commercial erbium-doped silica fibers fabricated through the MCVD and DND technologies," *IEEE J. Quantum Electron.*, vol. 49, no. 6, pp. 511–521, Jun. 2013.
[24] J. R. Lakowicz, *Principles of Fluorescence Spectroscopy*, 3rd ed. Baltimore, MD, USA: Springer-Verlag, 2006, pp. 157–204.
[25] A. D. Estrada and A. K. Dunn, "Improved sensitivity for two-photon frequency-domain lifetime measurement," *Opt. Exp.*, vol. 18, no. 13, pp. 13 631–13 639, Jun. 2010.